AIMS Mathematics, 10(7): 16692–16719.
DOI: 10.3934/math.2025749
Received: 19 May 2025
Revised: 05 July 2025
Accepted: 17 July 2025
Published: 24 July 2025

https://www.aimspress.com/journal/Math

Research article

Bifurcation analysis and the modulation instability in a nonlinear silica optical fibers

Maha Alammari[1], Muhammad Abuzar[2] and Solomon Manukure[3,*]

[1] Department of Mathematics, College of Science, King Saud University, P.O. Box 22452 Riyadh 11495, Saudi Arabia
[2] School of Mathematical Sciences, Guizhou Normal University, Guiyang, Yunyan 550003, China
[3] Department of Mathematics, Florida A&M University, Tallahassee, FL 32307, USA

* **Correspondence:** Email: solomon.manukure@famu.edu.

Abstract: The Schäfer-Wayne equation (SWE), a crucial model for ultrashort pulse propagation in nonlinear silicon optical fibers, is investigated using the F-expansion method and enhanced modified extended tanh expansion method (EMETEM). We derive diverse solitary wave solutions, including dark, bright, periodic, multi-peak periodic, and breather-like periodic solutions, visualized through $2D$ and $3D$ graphics. Novel contributions include comprehensive bifurcation analysis via planar dynamical systems revealing phase portrait classifications, modulation instability analysis for solution stability evaluation, and sensitivity analysis assessing parameter dependence and initial condition effects. The diverse solitary wave solutions represent a new advancement in understanding SWE dynamics. The study demonstrates the methods' robustness in examining nonlinear wave dynamics with applications in optics, engineering, and telecommunications.

Keywords: short pulse equation; analytical techniques; nonlinear waves; phase portraits; modulation instability; sensitive analysis; Schäfer-Wayne equation
Mathematics Subject Classification: 35C05, 35Q53

1. Introduction

Nonlinear partial differential equations (NLPDEs) are essential for modeling complex physical phenomena across various fields, including fluid mechanics, solid-state physics, and nonlinear optics [1, 2]. In optical communications, NLPDEs effectively describe soliton pulse propagation in fibers, where a balance between group-velocity dispersion and self-phase modulation leads to the formation of stable waveforms. This balance enables bright and dark solitons, depending on the dispersion regime, ensuring robust, distortion-free transmission in high-speed networks [3]. To

comprehend the qualitative and quantitative behavior of intricate physical systems, exact solutions to nonlinear partial differential equations are essential [4, 5]. Without only depending on numerical techniques, these solutions offer important insights into wave propagation, stability, and interaction dynamics. To build such solutions, a number of analytical approaches have been developed throughout time, including the sardar sub-equation, Kudryashov modified techniques, Hirota bilinear method, and Riccati's expanded simple equation approach [6, 7]. In both theoretical and applied contexts, exact solutions are crucial because they operate as standards for examining conserved quantities and evaluating numerical simulations.

Over the past few decades, temporal solitons have played a crucial role in nonlinear optics due to their ability to propagate over long distances without distortion, a result of the balance between dispersion and nonlinearity. These self-sustaining wave packets are foundational to modern optical communication systems, offering enhanced bandwidth and lower signal loss. The demand for exact analytical solutions to model soliton behavior has grown, as such solutions provide deeper insights into the dynamics of nonlinear systems [8, 9]. Solitons maintain their structure even during interactions, making them ideal for applications in fiber optics, ultrafast spectroscopy, and medical imaging [10, 11]. Recent developments in analytical techniques, such as the extended modified auxiliary equation mapping method [12], new auxiliary equation technique [13], modified Sardar sub-equation approach [14], unified Riccati equation expansion method [15], and Darboux transformation method [16, 17], have enabled exact solutions for a range of NLPDEs.

In the study of ultrashort pulse propagation in nonlinear optical media, the SW equation [18] has become an important model, particularly in cases when higher-order effects are not captured by conventional models, such as the nonlinear Schrödinger (NLS) equation. The complete wave character of ultrashort pulses is taken into account by SWE, which is more appropriate for femtosecond pulse regimes when dispersion and nonlinearity are no longer weak and separable than the NLS equation, which assumes slowly varying envelope approximations. Because of this, SWE can be used in next-generation fiber optic communication systems, where it is more important than ever to have strong nonlinear interactions, minimal dispersion, and ultra-fast data transfer. Furthermore, it is essential for laser system design, which allows for improved control over energy delivery, beam focusing, and pulse shaping in both industrial and research contexts [19]. Previous studies have explored the multi-component, semi-discrete, and time dependent complex coupled short pulse equation using Lie symmetry analysis as well as Darboux transformation methods to derive similarity solutions and complex solitons [20], and have introduced modified and nonlocal variants of the short pulse equation, constructing various soliton and breather solutions [21, 22].

There are still few analytical studies of SWE, despite its practical importance. Periodically and linearly stable solutions have been the subject of limited analytical research or numerical simulations in the majority of the literature to date [23–25]. These methods, however, frequently ignore the rich soliton structures and nonlinear dynamical complexity that SWE naturally possesses. Deeper comprehension of integrability, stability regimes, and bifurcation behavior under various physical factors is hampered by the absence of thorough analytical data. The gap identified in [26, 27] makes it possible to use advanced algebraic methods to find exact solutions, analyze bifurcation and modulation instability, and understand both the qualitative and quantitative behavior of solutions under realistic physical conditions. Closing this gap is crucial for improving real-world systems that depend on the dynamics of ultrashort optical pulses, as well as for expanding theoretical

understanding. Deriving several analytical closed-form solutions to the governing system is the main objective of this effort. Furthermore, we demonstrate the various wave profile dynamics of a few solitary wave solutions in $2D$, $3D$, and density graphics by numerical simulations. Nonetheless, the evolutionary dynamics of the solitary wave solutions that are achieved are fascinating and useful for complicated physical phenomena. The next sections provide a brief overview of the key characteristics of the EMETEM [28] and F-expansion method [29, 30] that will be employed in this work. Since they provide a variety of solutions to a particular physical model, EMETEM and the F-expansion strategy are superior options for studying NLPDEs.

The analytical methods, namely, the F-expansion method and the EMETEM, yield exact solutions efficiently, making it easier for researchers to explore the intricate behavior of nonlinear equations. Unlike traditional approaches, such as perturbation techniques, which often rely on linear approximations and thus lead to limited accuracy and solution scope, these newer strategies offer more robust alternatives. The EMEThEM framework enhances the classical tanh-function method by incorporating hyperbolic, trigonometric, and rational function solutions, effectively bridging shortcomings in earlier works, which did not provide detailed soliton structures. Additionally, the F-expansion technique proves to be a powerful tool for tackling a wide range of NLPDEs. It is especially well-suited for constructing meaningful and exact solutions, notably within fully integrable systems where nontrivial results are attainable. It is appropriate for recognizing simple wave structures in the SW model and requires minimal computing power. Additionally, we study the modulation instability, sensitivity, and bifurcation characteristics of the dynamical system [31, 32], examining parameter dependencies through planar dynamical system analysis. This combined method permits thorough characterization of the system's behavior. In the SW model, this makes EMETEM very useful for revealing new wave patterns and bifurcation structures. However, it requires more complex parameter adjustment and symbolic computing. Combining the two approaches thus provides a complementary benefit: EMETEM increases the variety and depth of accurate solutions, while the F-expansion method guarantees simplicity and speed.

Drawing upon the theoretical framework established above, this paper is organized as follows: Section 2 introduces the governing model and establishes its mathematical foundations. Section 3 presents a comprehensive exposition of the analytical methods employed, detailing their theoretical underpinnings and implementation strategies. Section 4 systematically derives and classifies the soliton solutions obtained through our methodological framework. Section 5 provides graphical representations of selected solutions, illustrating their dynamic behavior and characteristic properties under various parameter regimes. Section 6 gives an in-depth bifurcation analysis, examining the qualitative transitions in system behavior as control parameters vary. Section 7 investigates the modulation instability of the system, analyzing the conditions under which infinitesimal perturbations grow exponentially and lead to the formation of localized structures. In Section 8, the governing model's sensitivity analysis is covered in detail. Finally, Section 9 synthesizes our findings, discusses their physical significance and mathematical implications, and suggests promising directions for future research.

2. Governing model

An equation for short pulses (SP) is a fundamental representation in ultrashort pulse studies [33,34]. It is generally expressed as

$$\psi_{xt} = \alpha\psi + \frac{1}{3}\beta(\psi^3)_{xx}, \tag{2.1}$$

where $\psi = \psi(x,t)$ denotes the electric domain's strength. The parameters α and β characterize the system. This equation was first introduced by Schäfer with Wayne [35–37] to illustrate the transmission of ultra-short light pulses in silica optical fibers, which are used in sensors, telecommunications, and fiber lasers [38].

SPE can also be written in an alternative form:

$$\psi_{xt} = \alpha\psi + 2\beta\psi(\psi_x)^2 + \beta\psi^2\psi_{xx}. \tag{2.2}$$

This form highlights the nonlinear interactions within the system. When $\alpha = 1$ and $\beta = \frac{1}{2}$, the equation simplifies to

$$\psi_{xt} = \frac{1}{6}(\psi^3)_{xx}. \tag{2.3}$$

This special form of the SPE is particularly useful for analyzing the behavior of ultrashort pulses in nonlinear media.

The SPE is a substitute for the conventional method of modeling the movement of longer impulses, which is the cubic NLS problem. For shorter-duration pulses, whereby the band spectrum is not tightly confined to the carrier rate, the SPE is more precise. This makes the SPE particularly relevant for modern applications in nonlinear optics, where ultrashort pulses are increasingly important [39].

To explore the SW model's analytical findings, we employ the following transformation:

$$\psi(x,t) = N(\varsigma), \quad \varsigma = kx - ct + v, \tag{2.4}$$

where k, c, and v are constants. This transformation reduces the PDE to a nonlinear ordinary differential equation (NLODE):

$$(ck)N'' + \alpha N + 2k^2\beta N(N')^2 + \beta k^2 N^2 N'' = 0. \tag{2.5}$$

By balancing the highest-order terms in this equation, we can determine the appropriate form of the solution. Specifically, balancing N'' and N^2N'' or $N(N')^2$ suggests that the solution can be expressed in terms of a traveling wave.

To further simplify the analysis, we introduce the transformation $N(\varsigma) = \frac{1}{f(\varsigma)}$. Substituting this into Eq (2.5) yields

$$-ckf^3(\varsigma)f''(\varsigma) + 2ckf^2(\varsigma)(f'(\varsigma))^2 + \alpha f^4(\varsigma) + 4k^2\beta(f'(\varsigma))^2 - \beta k^2 f(\varsigma)f''(\varsigma) = 0. \tag{2.6}$$

Balancing the terms $f^4(\varsigma)$ and $f(\varsigma)f''(\varsigma)$ or $(f'(\varsigma))^2$ in Eq (2.6) confirms that the solution can be effectively described using this transformation.

This approach allows us to systematically derive the analytical solutions of the SWE and analyze their dynamical properties. The solutions obtained provide valuable insights into the behavior of ultrashort pulses in nonlinear media, contributing to a deeper understanding of the underlying physics.

3. Description of the methods

This section gives the detailed form of the applied analytical methods. Because of their shown ability to produce a large number of precise solutions for nonlinear evolution equations, the F-expansion method and EMETEM were selected. EMETEM provides more versatility and may provide a wider range of solution structures, such as exponential and rational forms; however, the F-expansion approach is favored for its ease of use and straightforward application to soliton and periodic solutions. These techniques support one another and offer a thorough analytical framework that is difficult to get using more conventional techniques like the sine-cosine or tanh-function procedures.

3.1. F- expansion method

We develop the mathematical structure needed for obtaining solitary wave solutions of the studied nonlinear phenomenon. The overall structure of NLPDEs may be stated in the following way:

$$\Psi(\psi, \psi_x, \psi_t, \psi_{xt}, \psi_{xx}, \cdots) = 0, \tag{3.1}$$

where Ψ represents a polynomial functional operating on partial derivatives. x represents a spatial parameter, and t illustrates the temporal value with regard to the waveforms $\psi = \psi(x, t)$. Consider the waveform:

$$\psi(x, t) = \Omega(\varsigma), \quad \varsigma = kx - ct + v. \tag{3.2}$$

The waveform that appears in this instance is ς, the wave amplitude being u, and the wave velocity as v. Therefore, Eq (3.2) becomes

$$F(\Omega, \Omega^{'}, \Omega^{''}, \Omega\Omega^{''}, \cdots) = 0. \tag{3.3}$$

Step 1: The simplified model verifies the solution's structure by consulting Eq (3.3):

$$f(\varsigma) = \sum_{i=0}^{N} B_i \Omega^i(\varsigma), \tag{3.4}$$

where

$$\Omega^{'}(\varsigma) = \sqrt{\alpha_1 \Omega^4(\varsigma) + \alpha_2 \Omega^2(\varsigma) + \alpha_3}\,. \tag{3.5}$$

The following is a description of the soliton wave profiles that come from Eq (3.5):

$$\begin{cases} \Omega(\varsigma) = \mathrm{sn}(\varsigma) = \tanh(\varsigma), \quad \alpha_1 \hookrightarrow m^2, \quad \alpha_2 \hookrightarrow -(1+m^2), \quad \alpha_3 \hookrightarrow 1, \quad m \to 1^-, \\ \Omega(\varsigma) = \mathrm{ns}(\varsigma) = \coth(\varsigma), \quad \alpha_1 \hookrightarrow 1, \quad \alpha_2 \hookrightarrow -(1+m^2), \quad \alpha_3 \hookrightarrow m^2, \quad m \to 1^-, \\ \Omega(\varsigma) = \mathrm{cn}(\varsigma) = \mathrm{sech}(\varsigma), \quad \alpha_1 \hookrightarrow -m^2, \quad \alpha_2 \hookrightarrow 2m^2-1, \quad \alpha_3 \hookrightarrow 1-m^2, \quad m \to 1^-, \\ \Omega(\varsigma) = \mathrm{ds}(\varsigma) = \mathrm{csch}(\varsigma), \quad \alpha_1 \hookrightarrow 1, \quad \alpha_2 \hookrightarrow 2m^2-1, \quad \alpha_3 \hookrightarrow -m^2(1-m^2), \quad m \to 1^-, \\ \Omega(\varsigma) = \mathrm{ns}(\varsigma) \pm \mathrm{ds}(\varsigma) = \coth(\varsigma) \pm \mathrm{csch}(\varsigma), \quad \alpha_1 \hookrightarrow \frac{1}{4}, \quad \alpha_2 \hookrightarrow \frac{m^2-2}{2}, \quad \alpha_3 \hookrightarrow \frac{m^2}{4}, \quad m \to 1^-, \\ \Omega(\varsigma) = \mathrm{sn}(\varsigma) \pm \mathrm{icn}(\varsigma) = \tanh(\varsigma) \pm \mathrm{i}\,\mathrm{sech}(\varsigma), \quad \alpha_1 \hookrightarrow \frac{m^2}{4}, \quad \alpha_2 \hookrightarrow \frac{m^2-2}{2}, \quad \alpha_3 \hookrightarrow \frac{m^2}{4}, \quad m \to 1^-, \\ \Omega(\varsigma) = \frac{\mathrm{sn}(\varsigma)}{1\pm\mathrm{dn}(\varsigma)} = \frac{\tanh(\varsigma)}{1\pm\mathrm{sech}}, \quad \alpha_1 \hookrightarrow \frac{m^2}{4}, \quad \alpha_2 \hookrightarrow \frac{m^2-2}{2}, \quad \alpha_3 \hookrightarrow \frac{m^2}{4}, \quad m \to 1^-. \end{cases} \tag{3.6}$$

The Jacobi elliptic functions $\mathrm{sn}(\varsigma)$, $\mathrm{ns}(\varsigma)$, $\mathrm{cn}(\varsigma)$, $\mathrm{ds}(\varsigma)$, and $\mathrm{dn}(\varsigma)$ fit modulus $0 < m < 1$ in this instance. The balancing method in Eq (3.2) gives the constants B_i, where i goes from 0 to N.

Step 2: Using Eqs (3.4) and (3.5) in Eq (3.2) gives a set of equations that helps find the unknown parameters in Eqs (3.2)–(3.5).

3.2. EMETEM

In this section, the outline of the steps involved in utilizing the EMETEM to deal with NLPDEs is discussed. The solution of the Eq (2.6) for the EMETEM has the form

$$f(\varsigma) = \mathcal{R}_0 + \sum_{k=1}^{\varpi} \mathcal{R}_k[\Omega(\varsigma)]^k + \sum_{k=1}^{\varpi} \mathcal{S}_k[\Omega(\varsigma)]^{-k}, \tag{3.7}$$

where

$$\frac{d}{d\varsigma}\Omega(\varsigma) = L + [\Omega(\varsigma)]^2. \tag{3.8}$$

The positive integer ϖ is determined by employing the homogeneous balancing principle on Eq (2.6). Substitution of Eqs (3.7) and (3.8) into Eq (2.6) yields a polynomial in $\Omega(\varsigma)$, and equating each term of the polynomial to zero leads to a system of algebraic equations. The solution of these equations assigns real values to the constants $\mathcal{R}_0, \mathcal{R}_1, \mathcal{R}_2, ..., \mathcal{R}_k, \mathcal{S}_1, \mathcal{S}_2, ..., \mathcal{S}_k$ that cannot simultaneously be zero.

Eq (3.8) has the following general solutions.

Case 1: When $L < 0$,

$$\Omega_1(\varsigma) = -\sqrt{-L}\tanh[\sqrt{-L}\varsigma], \tag{3.9}$$

$$\Omega_2(\varsigma) = -\sqrt{-L}\coth[\sqrt{-L}\varsigma], \tag{3.10}$$

$$\Omega_3(\varsigma) = -\sqrt{-L}\left(\tanh[2\sqrt{-L}\varsigma] + i\omega\,\mathrm{sech}[2\sqrt{-L}\varsigma]\right), \tag{3.11}$$

$$\Omega_4(\varsigma) = \frac{L - \sqrt{-L}\tanh[\sqrt{-L}\varsigma]}{1 + \sqrt{-L}\tanh[\sqrt{-L}\varsigma]}, \tag{3.12}$$

$$\Omega_5(\varsigma) = \frac{\sqrt{-L}(5 - 4\cosh[2\sqrt{-L}\varsigma])}{3 + 4\sinh[2\sqrt{-L}\varsigma]}, \tag{3.13}$$

$$\Omega_6(\varsigma) = \frac{\omega\sqrt{-L(m^2+n^2)} - m\sqrt{-L}\cosh[2\sqrt{-L}\varsigma]}{m\sinh[2\sqrt{-L}\varsigma] + n}, \tag{3.14}$$

$$\Omega_7(\varsigma) = \omega\sqrt{-L}\left(1 - \frac{2m}{m + \cosh[2\sqrt{-L}\varsigma] - \omega\sinh[2\sqrt{-L}\varsigma]}\right). \tag{3.15}$$

Case 2: When $L > 0$,

$$\Omega_8(\varsigma) = \sqrt{L}\tan[\sqrt{L}\varsigma], \tag{3.16}$$

$$\Omega_9(\varsigma) = -\sqrt{L}\cot[\sqrt{L}\varsigma], \tag{3.17}$$

$$\Omega_{10}(\varsigma) = \sqrt{L}\left(\tan[2\sqrt{L}\varsigma] + \omega\sec[2\sqrt{L}\varsigma]\right), \tag{3.18}$$

$$\Omega_{11}(\varsigma) = -\sqrt{L}\left(\frac{1 - \tan[\sqrt{L}\varsigma]}{1 + \tan[\sqrt{L}\varsigma]}\right), \tag{3.19}$$

$$\Omega_{12}(\varsigma) = -\sqrt{L}\left(\frac{(4 - 5\cos[2\sqrt{L}\varsigma])}{3 + 5\sin[2\sqrt{L}\varsigma]}\right), \tag{3.20}$$

$$\Omega_{13}(\varsigma) = \frac{\omega\sqrt{L(m^2-n^2)} - m\sqrt{L}\cos[2\sqrt{L}\varsigma]}{m\sin[2\sqrt{L}\varsigma] + n}, \tag{3.21}$$

$$\Omega_{14}(\varsigma) = i\omega\sqrt{L}\left(1 - \frac{2m}{m + \cos[2\sqrt{L}\varsigma] - i\omega\sin[2\sqrt{L}\varsigma]}\right). \tag{3.22}$$

Case 3: When $L = 0$,

$$\Omega_{15}(\varsigma) = -\frac{1}{\varsigma}. \tag{3.23}$$

4. Extraction of analytical solutions

In this section, the analytical methods will be applied to the model provided to extricate the different types of soliton solutions.

4.1. F- expansion method

Applying the solution as

$$f(\varsigma) = B_0 + B_1\Omega(\varsigma), \tag{4.1}$$

the following formulations are obtained by substituting Eqs (4.1) and (3.5) into Eq (2.6):

$$\Omega(\varsigma)^0 = 2\alpha_3 ckB_0^2B_1^2 + 4\alpha_3\beta k^2B_1^2 + \alpha B_0^4 = 0,$$

$$\begin{aligned}
\Omega(\varsigma)^1 &= -\alpha_2\alpha_2 ckB_0^3B_1 + 4\alpha_3 ckB_0B_1^3 - \alpha_2\beta k^2B_0B_1 + 4\alpha B_0^3B_1 = 0,\\
\Omega(\varsigma)^2 &= -3cB_0^2B_1^2\alpha_2 k + 2\left(\alpha_2 cB_0^2B_1^2 + \alpha_3 cB_1^4\right)k + 6\alpha B_0^2B_1^2 + 3\beta B_1^2\alpha_2 k^2 = 0,\\
\Omega(\varsigma)^3 &= -\left(2\alpha_1 cB_0^3B_1 + 3\alpha_2 cB_0B_1^3\right)k + 4cB_0B_1^3\alpha_2 k + 4\alpha B_0B_1^3 - 2\beta B_0B_1\alpha_1 k^2 = 0,\\
\Omega(\varsigma)^4 &= -\left(6\alpha_1 cB_0^2B_1^2 + \alpha_2 cB_1^4\right)k + 2\left(\alpha_1 cB_0^2B_1^2 + \alpha_2 cB_1^4\right)k + \alpha B_1^4 + 2\beta B_1^2\alpha_1 k^2 = 0,\\
\Omega(\varsigma)^5 &= -2cB_0B_1^3\alpha_1 k = 0.
\end{aligned} \tag{4.2}$$

The system of equations is solved to obtain the following results:

$$c = \frac{3\alpha_2\alpha}{k\left(4\alpha_1\alpha_3 - 3\alpha_2^2\right)}, \quad B_0 = 0, \quad B_1 = \sqrt{-\frac{\left(4\alpha_1\alpha_3\beta - 3\alpha_2^2\beta\right)}{2a\alpha_1}}. \tag{4.3}$$

Substituting the expression from Eq (4.3) into Eq (4.1), while simultaneously incorporating the constraints established by Eq (3.6), we perform a systematic analytical reduction. A thorough study shows that the sign of the expression inside the radical plays a crucial role in guaranteeing real-valued solutions for the given term, which involves a square root. When $4\alpha_1 < 3\alpha_3\beta$, real solutions are obtained for the normal physical restrictions of silica fibers where $\alpha > 0$ and $\beta > 0$. This procedure yields the exact form of the soliton solutions, which can be classified into the following distinct categories based on their mathematical structure and physical characteristics.

Case 1: When $\Omega(\varsigma) = \mathrm{sn}(\varsigma) = \tanh(\varsigma)$, $\alpha_1 = m^2$, $\alpha_2 = -(1+m^2)$, $\alpha_3 = 1$.

$$f_{1,1}(x,t) = -\sqrt{-\frac{\left(4\alpha_1\alpha_3\beta - 3\alpha_2^2\beta\right)}{2\alpha_3\alpha}}\, k \tanh\left(\frac{3\alpha_2\alpha t}{k\left(4\alpha_1\alpha_3 - 3\alpha_2^2\right)} - kx - v\right). \tag{4.4}$$

Case 2: $\Omega(\varsigma) = \mathrm{ns}(\varsigma) = \coth(\varsigma)$, $\alpha_1 = 1$, $\alpha_2 = -(1+m^2)$, $\alpha_3 = m^2$.

$$f_{2,1}(x,t) = -\sqrt{-\frac{\left(4\alpha_1\alpha_3\beta - 3\alpha_2^2\beta\right)}{2\alpha_3\alpha}}\, k \coth\left(\frac{3\alpha_2\alpha t}{k\left(4\alpha_1\alpha_3 - 3\alpha_2^2\right)} - kx - v\right). \tag{4.5}$$

Case 3: $\Omega(\varsigma) = \mathrm{cn}(\varsigma) = \mathrm{sech}(\varsigma)$, $\alpha_1 = -m^2$, $\alpha_2 = 2m^2 - 1$, $\alpha_3 = 1 - m^2$.

$$f_{3,1}(x,t) = \sqrt{-\frac{\left(4\alpha_1\alpha_3\beta - 3\alpha_2^2\beta\right)}{2\alpha_3\alpha}}\, k\, \mathrm{sech}\left(\frac{3\alpha_1\alpha t}{k\left(4\alpha_1\alpha_3 - 3\alpha_2^2\right)} - kx - v\right). \tag{4.6}$$

Case 4: $\Omega(\varsigma) = \mathrm{ds}(\varsigma) = \mathrm{csch}(\varsigma)$, $\alpha_1 = 1$, $\alpha_2 = 2m^2 - 1$, $\alpha_3 = -m^2(1-m^2)$.

$$f_{4,1}(x,t) = \frac{\sqrt{2}\,\sqrt{-\frac{4\beta\left(\alpha_1\alpha_3 - \frac{3\alpha_2^2}{4}\right)}{\alpha_3\alpha}}\, k}{2\sinh\left(\frac{4(kx+v)\left(\alpha_1\alpha_3 - \frac{3\alpha_2^2}{4}\right)k - 3\alpha_2\alpha t}{k\left(4\alpha_1\alpha_3 - 3\alpha_2^2\right)}\right)}. \tag{4.7}$$

Case 5: $\Omega(\varsigma) = \mathrm{ns}(\varsigma) \pm \mathrm{ds}(\varsigma) = \coth(\varsigma) \pm \mathrm{csch}(\varsigma)$, $\alpha_1 = \frac{1}{4}$, $\alpha_2 = \frac{m^2-2}{2}$, $\alpha_3 = \frac{m^2}{4}$.

$$f_{5,1}(x,t) = \frac{\sqrt{-\frac{2\left(4\alpha_1\alpha_3\beta-3\alpha_2^2 b\right)}{\alpha_3\alpha}}\, k\left(-\coth\left(\frac{3\alpha_2 at}{k\left(4\alpha_1\alpha_3-3\alpha_2^2\right)}-kx-v\right)-\mathrm{csch}\left(\frac{3\alpha_2\alpha t}{k\left(4\alpha_1\alpha_3-3\alpha_2^2\right)}-kx-v\right)\right)}{2}, \tag{4.8}$$

$$f_{5,2}(x,t) = \frac{\sqrt{-\frac{2\left(4\alpha_1\alpha_3\beta-3\alpha_2^2\beta\right)}{\alpha_3\alpha}}\, k\left(-\coth\left(\frac{3\alpha_2\alpha t}{k\left(4\alpha_1\alpha_3-3\alpha_2^2\right)}-kx-v\right)+\mathrm{csch}\left(\frac{3\alpha_2\alpha t}{k\left(4\alpha_1\alpha_3-3\alpha_2^2\right)}-kx-v\right)\right)}{2}. \tag{4.9}$$

Case 6: $\Omega(\varsigma) = \mathrm{sn}(\varsigma) \pm \mathrm{icn}(\varsigma) = \tanh(\varsigma) \pm i\,\mathrm{sech}(\varsigma)$, $\alpha_1 = \frac{m^2}{4}$, $\alpha_2 = \frac{m^2-2}{2}$, $\alpha_3 = \frac{m^2}{4}$.

$$f_{6,1}(x,t) = \frac{\sqrt{-\frac{2\left(4\alpha_1\alpha_3\beta-3\alpha_2^2\beta\right)}{\alpha_3\alpha}}\, k\left(-\tanh\left(\frac{3\alpha_2\alpha t}{k\left(4\alpha_1\alpha_3-3\alpha_2^2\right)}-kx-v\right)+i\,\mathrm{sech}\left(\frac{3\alpha_2\alpha t}{k\left(4\alpha_1\alpha_3-3\alpha_2^2\right)}-kx-v\right)\right)}{2}, \tag{4.10}$$

$$f_{6,2}(x,t) = \frac{\sqrt{-\frac{2\left(4\alpha_1\alpha_3\beta-3\alpha_2^2\beta\right)}{\alpha_3\alpha}}\, k\left(-\tanh\left(\frac{3\alpha_2\alpha t}{k\left(4\alpha_1\alpha_3-3\alpha_2^2\right)}-kx-v\right)-i\,\mathrm{sech}\left(\frac{3\alpha_2\alpha t}{k\left(4\alpha_1\alpha_3-3\alpha_2^2\right)}-kx-v\right)\right)}{2}. \tag{4.11}$$

Case 7: $\Omega(\varsigma) = \frac{\mathrm{sn}(\varsigma)}{1\pm\mathrm{dn}(\varsigma)} = \frac{\tanh(\varsigma)}{1\pm\mathrm{sech}}$, $\alpha_1 = \frac{m^2}{4}$, $\alpha_2 = \frac{m^2-2}{2}$, $\alpha_3 = \frac{m^2}{4}$.

$$f_{7,1}(x,t) = -\frac{\sqrt{-\frac{2\left(4\alpha_1\alpha_3\beta-3\alpha_2^2\beta\right)}{\alpha_3\alpha}}\, k\tanh\left(\frac{3\alpha_2\alpha t}{k\left(4\alpha_1\alpha_3-3\alpha_2^2\right)}-kx-v\right)}{2\left(1+\mathrm{sech}\left(\frac{3\alpha_2\alpha t}{n\left(4\alpha_1\alpha_3-3\alpha_2^2\right)}-kx-v\right)\right)}, \tag{4.12}$$

$$f_{7,2}(x,t) = \frac{\sqrt{-\frac{2\left(4\alpha_1\alpha_3\beta-3\alpha_2^2\beta\right)}{\alpha_3\alpha}}\, k\tanh\left(\frac{3\alpha_2\alpha t}{k\left(4\alpha_1\alpha_3-3\alpha_2^2\right)}-kx-v\right)}{2\left(1-\mathrm{sech}\left(\frac{3\alpha_2\alpha t}{k\left(4\alpha_1\alpha_3-3\alpha_2^2\right)}-kx-v\right)\right)}. \tag{4.13}$$

4.2. EMETEM

For the case where $\varpi = 1$, Eq (3.7) assumes the simplified form:

$$f(\varsigma) = \mathcal{R}_0 + \mathcal{R}_1[\Omega(\varsigma)] + \mathcal{S}_1[\Omega(\varsigma)]^{-1}. \tag{4.14}$$

When we substitute Eq (4.14) along with Eq (3.8) into the governing Eq (2.6), we obtain a polynomial expression in terms of $\Omega(\varsigma)$. By applying the principle of homogeneous balance and setting each coefficient of this polynomial to zero, we derive a system of algebraic equations. Solving this system yields the following parameter constraints:

$$R_0 = 0, \quad S_1 = LR_1, \quad \beta = 0, \quad c = \frac{\alpha}{4kL}. \tag{4.15}$$

Although $\beta = 0$ linearizes the model, we consider it as an illustrative special case. The general case with $\beta \neq 0$ may be explored to preserve nonlinear characteristics in future work. By incorporating

these parameter values into Eq (4.15) and applying the transformation defined in Eq (3.8), we obtain the following family of solitary wave solutions to the SWE:

Case 1: When $L < 0$,

$$f_1(x,t) = -\sqrt{-L}R_1 \tanh\left(\sqrt{-L}\left(-\frac{\alpha t}{4kL} + kx + v\right)\right) - \frac{LR_1 \coth\left(\sqrt{-L}\left(-\frac{\alpha t}{4kL} + kx + v\right)\right)}{\sqrt{-L}}, \tag{4.16}$$

$$f_2(x,t) = \left(-\sqrt{-L}\right)R_1 \coth\left(\sqrt{-L}\left(-\frac{\alpha t}{4kL} + kx + v\right)\right) - \frac{LR_1 \tanh\left(\sqrt{-L}\left(-\frac{\alpha t}{4kL} + kx + v\right)\right)}{\sqrt{-L}}, \tag{4.17}$$

$$\begin{aligned} f_3(x,t) = &-\frac{LR_1}{\sqrt{-L}\left(\tanh\left(2\sqrt{-L}\left(-\frac{\alpha t}{4kL} + kx + v\right)\right) + i\omega \operatorname{sech}\left(2\sqrt{-L}\left(-\frac{\alpha t}{4kL} + kx + v\right)\right)\right)} - \\ &\sqrt{-L}R_1\left(\tanh\left(2\sqrt{-L}\left(-\frac{\alpha t}{4kL} + kx + v\right)\right) + i\omega \operatorname{sech}\left(2\sqrt{-L}\left(-\frac{\alpha t}{4kL} + kx + v\right)\right)\right), \end{aligned} \tag{4.18}$$

$$f_4(x,t) = \frac{LR_1\left(\sqrt{-L}\tanh\left(\sqrt{-L}\left(-\frac{\alpha t}{4kL} + kx + v\right)\right) + 1\right)}{L - \sqrt{-L}\tanh\left(\sqrt{-L}\left(-\frac{\alpha t}{4kL} + kx + v\right)\right)} + \frac{R_1\left(L - \sqrt{-L}\tanh\left(\sqrt{-L}\left(-\frac{\alpha t}{4kL} + kx + v\right)\right)\right)}{\sqrt{-L}\tanh\left(\sqrt{-L}\left(-\frac{\alpha t}{4kL} + kx + v\right)\right) + 1}, \tag{4.19}$$

$$f_5(x,t) = \frac{LR_1\left(4\sinh\left(2\sqrt{-L}\left(-\frac{\alpha t}{4kL} + kx + v\right)\right) + 3\right)}{\sqrt{-L}\left(5 - 4\cosh\left(2\sqrt{-L}\left(-\frac{\alpha t}{4kL} + kx + v\right)\right)\right)} + \frac{\sqrt{-L}R_1\left(5 - 4\cosh\left(2\sqrt{-L}\left(-\frac{\alpha t}{4kL} + kx + v\right)\right)\right)}{4\sinh\left(2\sqrt{-L}\left(-\frac{\alpha t}{4kL} + kx + v\right)\right) + 3}, \tag{4.20}$$

$$\begin{aligned} f_6(x,t) = &\frac{R_1\left(\omega\sqrt{-L\left(m^2+n^2\right)} - \sqrt{-L}m\cosh\left(2\sqrt{-L}\left(-\frac{\alpha t}{4kL} + kx + v\right)\right)\right)}{m\sinh\left(2\sqrt{-L}\left(-\frac{\alpha t}{4kL} + kx + v\right)\right) + n} + \\ &\frac{LR_1\left(m\sinh\left(2\sqrt{-L}\left(-\frac{\alpha t}{4kL} + kx + v\right)\right) + n\right)}{\omega\sqrt{-L\left(m^2+n^2\right)} - \sqrt{-L}m\cosh\left(2\sqrt{-L}\left(-\frac{\alpha t}{4kL} + kx + v\right)\right)}, \end{aligned} \tag{4.21}$$

$$\begin{aligned} f_7(x,t) = &\sqrt{-L}R_1\omega\left(1 - \frac{2m}{-\omega\sinh\left(2\sqrt{-L}\left(-\frac{\alpha t}{4kL} + kx + v\right)\right) + \cosh\left(2\sqrt{-L}\left(-\frac{\alpha t}{4kL} + kx + v\right)\right) + m}\right) \\ &+\frac{LR_1}{\sqrt{-L}\omega\left(1 - \frac{2m}{-\omega\sinh\left(2\sqrt{-L}\left(-\frac{\alpha t}{4kL} + kx + v\right)\right) + \cosh\left(2\sqrt{-L}\left(-\frac{\alpha t}{4kL} + kx + v\right)\right) + m}\right)}. \end{aligned} \tag{4.22}$$

Case 2: When $L > 0$,

$$f_8(x,t) = \sqrt{L}R_1 \tan\left(\sqrt{L}\left(-\frac{\alpha t}{4kL} + kx + v\right)\right) + \sqrt{L}R_1 \cot\left(\sqrt{L}\left(-\frac{\alpha t}{4kL} + kx + v\right)\right), \tag{4.23}$$

$$f_9(x,t) = \left(-\sqrt{L}\right) R_1 \cot\left(\sqrt{L}\left(-\frac{\alpha t}{4kL} + kx + v\right)\right) - \sqrt{L} R_1 \tan\left(\sqrt{L}\left(-\frac{\alpha t}{4kL} + kx + v\right)\right), \tag{4.24}$$

$$f_{10}(x,t) = \frac{\sqrt{L} R_1}{\omega \sec\left(2\sqrt{L}\left(-\frac{\alpha t}{4kL} + kx + v\right)\right) + \tan\left(2\sqrt{L}\left(-\frac{\alpha t}{4kL} + kx + v\right)\right)} + \sqrt{L} R_1 \left(\omega \sec\left(2\sqrt{L}\left(-\frac{\alpha t}{4kL} + kx + v\right)\right) + \tan\left(2\sqrt{L}\left(-\frac{\alpha t}{4kL} + kx + v\right)\right)\right), \tag{4.25}$$

$$f_{11}(x,t) = -\frac{\sqrt{L} R_1 \left(1 - \tan\left(\sqrt{L}\left(-\frac{\alpha t}{4kL} + kx + v\right)\right)\right)}{\tan\left(\sqrt{L}\left(-\frac{\alpha t}{4kL} + kx + v\right)\right) + 1} - \frac{\sqrt{L} R_1 \left(\tan\left(\sqrt{L}\left(-\frac{\alpha t}{4kL} + kx + v\right)\right) + 1\right)}{1 - \tan\left(\sqrt{L}\left(-\frac{\alpha t}{4kL} + kx + v\right)\right)}, \tag{4.26}$$

$$f_{12}(x,t) = -\frac{\sqrt{L} R_1 \left(5\sin\left(2\sqrt{L}\left(-\frac{\alpha t}{4kL} + kx + v\right)\right) + 3\right)}{4 - 5\cos\left(2\sqrt{L}\left(-\frac{\alpha t}{4kL} + kx + v\right)\right)} - \frac{\sqrt{L} R_1 \left(4 - 5\cos\left(2\sqrt{L}\left(-\frac{\alpha t}{4kL} + kx + v\right)\right)\right)}{5\sin\left(2\sqrt{L}\left(-\frac{\alpha t}{4kL} + kx + v\right)\right) + 3}, \tag{4.27}$$

$$f_{13}(x,t) = \frac{L R_1 \left(m\sin\left(2\sqrt{L}\left(-\frac{\alpha t}{4kL} + kx + v\right)\right) + n\right)}{\omega\sqrt{L\left(m^2 - n^2\right)} - \sqrt{L} m \cos\left(2\sqrt{L}\left(-\frac{\alpha t}{4kL} + kx + v\right)\right)} + \frac{R_1 \left(\omega\sqrt{L\left(m^2 - n^2\right)} - \sqrt{L} m \cos\left(2\sqrt{L}\left(-\frac{\alpha t}{4kL} + kx + v\right)\right)\right)}{m\sin\left(2\sqrt{L}\left(-\frac{\alpha t}{4kL} + kx + v\right)\right) + n}, \tag{4.28}$$

$$f_{14}(x,t) = -\frac{i\sqrt{L} R_1}{\omega\left(1 - \frac{2m}{-i\omega\sin\left(2\sqrt{L}\left(-\frac{\alpha t}{4kL} + kx + v\right)\right) + \cos\left(2\sqrt{L}\left(-\frac{\alpha t}{4kL} + kx + v\right)\right) + m}\right)} + i\sqrt{L} R_1 \omega \left(1 - \frac{2m}{-i\omega\sin\left(2\sqrt{L}\left(-\frac{\alpha t}{4kL} + kx + v\right)\right) + \cos\left(2\sqrt{L}\left(-\frac{\alpha t}{4kL} + kx + v\right)\right) + m}\right). \tag{4.29}$$

Case 3: When $L = 0$,

$$f_{15}(x,t) = L R_1 \left(-\frac{\alpha t}{4kL} - kx - v\right) - \frac{R_1}{-\frac{\alpha t}{4kL} + kx + v}. \tag{4.30}$$

5. Graphical analysis

The SW equation holds significant importance for modeling weakly dispersive, unidirectional, and weakly nonlinear wave propagation. Graphically, it provides insightful representations of complex wave phenomena, including wave steepening and soliton formation, highlighting the delicate balance between nonlinearity and dispersion in physical systems. These visual representations are essential for analyzing wave dynamics in shallow water environments and optical media. The characteristic profiles of waves in the governing model are fundamentally determined by the specific parameter

values employed. Solution functions derived through both the F-expansion method (4.4)–(4.13) and EMETEM (4.16)–(4.30) exhibit diverse forms contingent upon free parameter values, which directly influence the wave velocity c. These parameters correlate with the coefficient of the highest power in both linear and nonlinear terms of Eq (2.6). The solution functions developed in Section 4 are visualized through multiple graphical representations. The primary objective of this investigation is to identify precise soliton solutions for the SWE.

Figure 1 illustrates the dark behavior of Eq (4.4) with parameters $k = 0.5$, $a = 0.1$, $b = -2$, $v = 0.5$, and $c = 0.2$. Bright solitons in Figure 2 (e.g., Eq (4.6)) emerge under $\alpha > 0$, $\beta > 0$, and $k > 0$, consistent with anomalous dispersion. Similarly, dark solitons such as Eq (4.4) also arise under $\alpha > 0$ and $k > 0$, although with $\beta = 0$, confirming their coexistence within related parameter regimes.

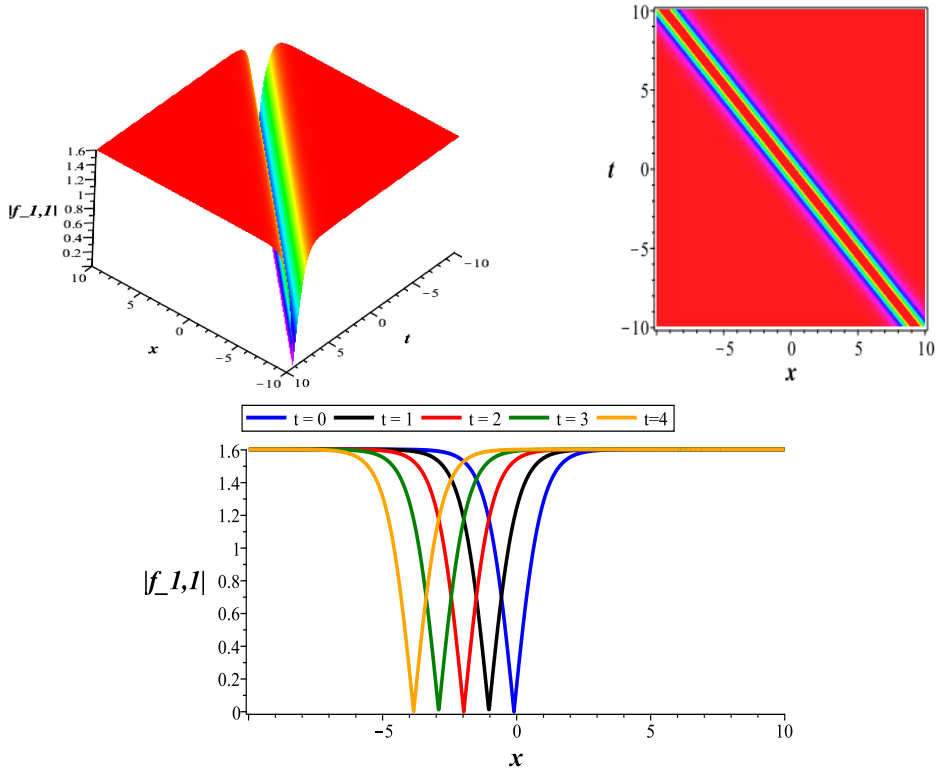

Figure 1. Graphical representation of the solution $f_{1,1}(x, t)$ given by Eq (4.4), which shows the dark soliton solution using the parametric values $m = 0.3$, $\alpha = 0.3$, $\beta = 0.5$, $k = 1$, and $v = 0.1$.

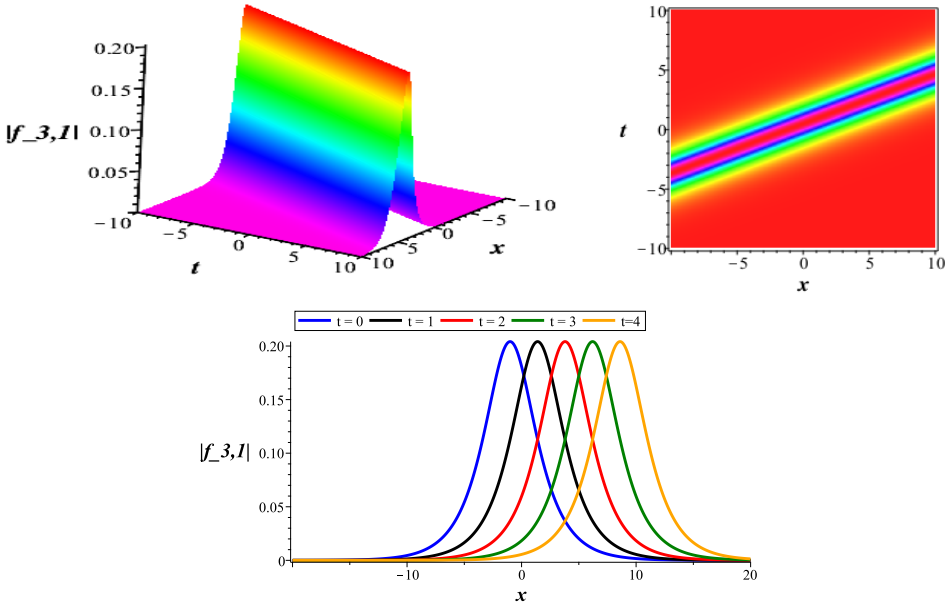

Figure 2. Graphical representation of the solution $f_{3,1}(x,t)$ given by Eq (4.6), which shows the bright soliton solution using the parametric values $m = 0.5$, $\alpha = 0.6$, $\beta = 0.1$, and $k = v = 0.5$.

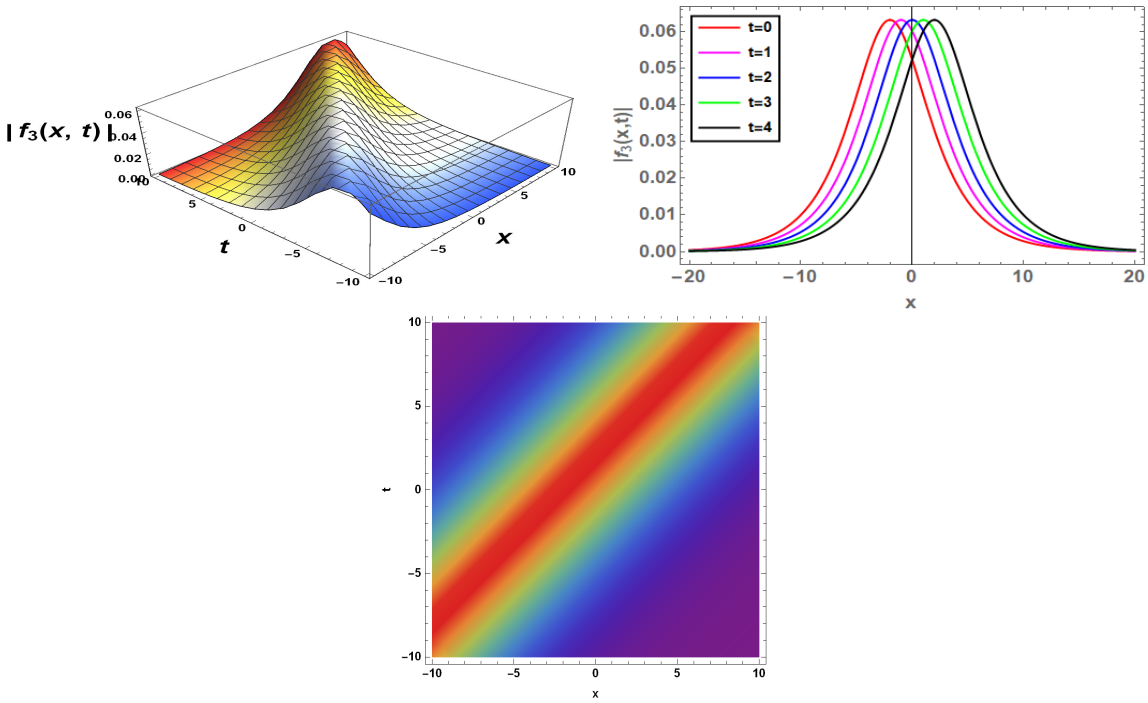

Figure 3. The bright solitary wave profile plotted shows the sech-shaped envelope of the solution $f_3(x,t)$ to the governing equation, taking the values $k = 0.5$, $\alpha = 0.1$, $R_1 = -0.1$, $\omega = 1$ $L = -0.1$, and $v = 1$. The soliton maintains its shape during propagation due to the balance between dispersion and nonlinearity.

Figure 3 displays the spatial profile of a bright soliton, characterized by a localized bell-shaped amplitude distribution, with parameters $L = -0.1$, $v = 1$, $k = 0.5$, $\alpha = 0.1$, $R_1 = -0.1$, and $\omega = 0.01$. Figure 4 depicts the soliton solution for $f_7(x,t)$ with parameter values $L = -0.2$, $v = 1$, $k = 0.5$, $\alpha = 0.3$, $R_1 = -0.1$, $\omega = 0.01$, and $m = -0.6$.

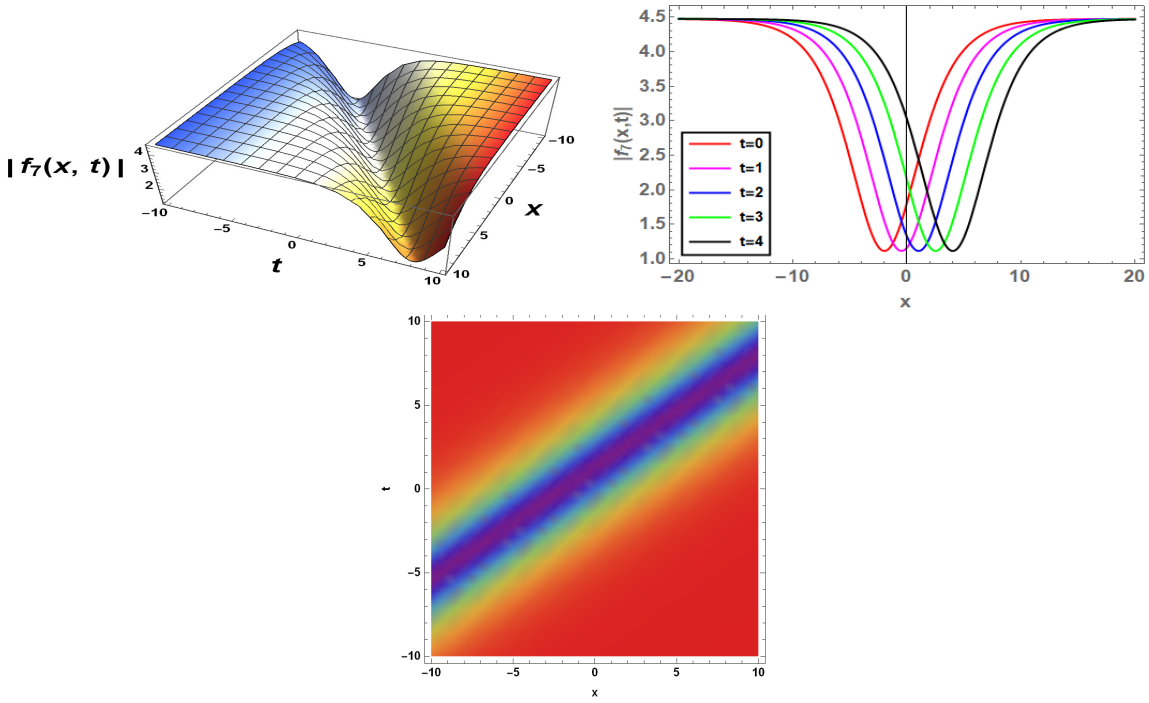

Figure 4. Spatial profile of a dark soliton exhibiting a localized intensity dip on a non-zero background by considering the perimetric values as $k = 0.5$, $\alpha = 0.3$, $R_1 = -0.1$, $\omega = 0.01$, $L = 0.2$, and $v = 1$. The solution corresponds to the defocusing discussed model and is characterized by a phase jump across the soliton minimum.

The function $f_8(x,t)$ exhibits singular periodic behavior as illustrated in Figure 5, utilizing parameters $L = -0.2$, $v = 1$, $k = 0.5$, $\alpha = 0.3$, $R_1 = -0.1$, and $\omega = 0.01$. In contrast to standard periodic or soliton solutions, these singular periodic structures demonstrate amplitude divergence at specific points while maintaining overall periodicity. Figure 6 illustrates $f_{13}(x,t)$, displaying a localized, multi-peak, spiky structure that emerges from and subsequently returns to a relatively flat background. The wave's symmetry and multi-peak profile identify it as a higher-order Peregrine-type rogue wave rather than a conventional soliton, with parameters $L = 1$, $v = 1$, $k = 0.5$, $\alpha = 1$, $R_1 = 1$, $\omega = 0.4$, $m = 0.3$, and $n = 0.4$. The spatial profile at various time snapshots is displayed in the plot. A stable periodic structure is shown by the peaks' endurance throughout time. This implies properties of brilliant soliton trains, perhaps with internal phase modulation, as the wave profiles stay confined and reoccur.

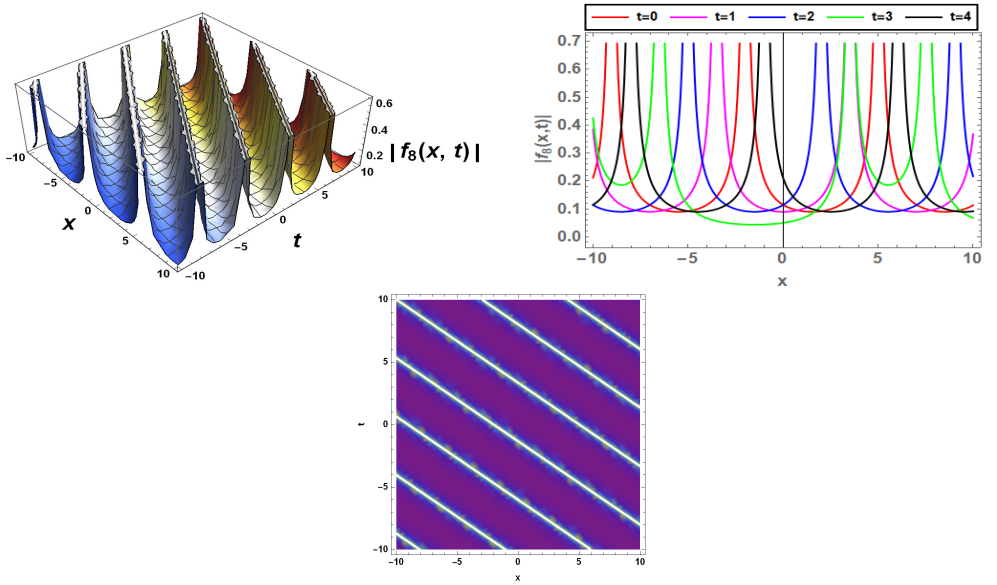

Figure 5. Singular periodic solution of the governing nonlinear equation exhibiting periodic waveforms with localized singularities, with parameter values $L = -0.2$, $v = 1$, $k = 0.5$, $\alpha = 0.3$, $R_1 = -0.1$, and $\omega = 0.01$. The solution retains a repeating structure despite the divergence of amplitude at isolated points.

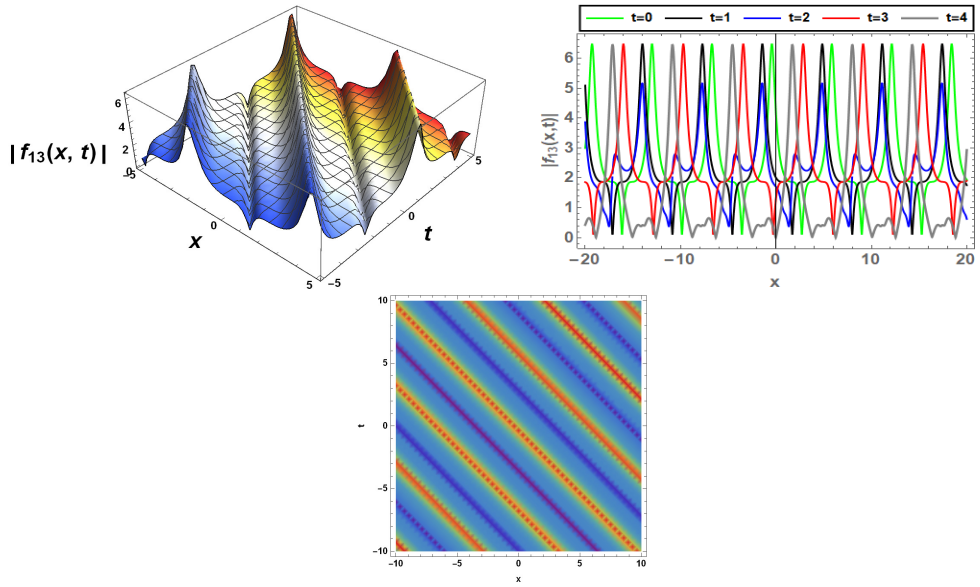

Figure 6. $3D$ plot of the absolute value of a higher-order rational solution $f_{13}(x,t)$ to the SWE. The solution displays strong spatiotemporal localization and steep amplitude peaks, indicative of a breather-type or multi-peak periodic soliton, with parameters $L = 1$, $v = 1$, $k = 0.5$, $\alpha = 1$, $R_1 = 1$, $\omega = 0.4$, $m = 0.3$, and $n = 0.4$. These structures emerge transiently and vanish without leaving behind permanent changes in the wave profile.

Figure 7 presents $f_{14}(x,t)$ with parameters $L = 1$, $v = 1$, $k = 0.5$, $\alpha = 0.5$, $R_1 = 0.3$, $\omega = 0.4$, $m = 0.5$, and $n = 0.5$, revealing more intricate interference patterns and extended side lobes compared

to lower-order rogue waves, suggesting a nonlinear superposition of multiple fundamental rogue wave modes. Energy localization and transfer, which are characteristic of breather-type waves, where energy periodically concentrates and redistributes in nonlinear systems, are also hinted at by the amplitude modulation over time. Such phenomenon, which suggests a nonlinear interaction between dispersion and nonlinearity, is frequently observed in fluid dynamics, nonlinear optics, and plasma physics. A comparison of the current study with recently published studies on the same governing model is shown in the Table 1. It draws attention to the unique analytical techniques, kinds of solutions, and thorough analyses used in our work. This comparison highlights the uniqueness and breadth of the present study.

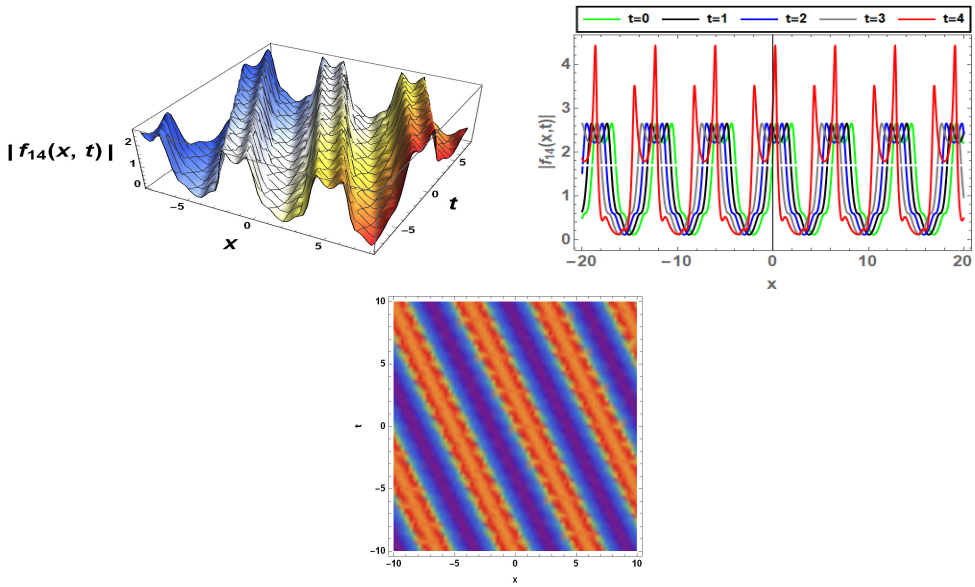

Figure 7. 3*D* plot of a higher-order rational solution to SWE exhibiting multiple sharp peaks and localized spatiotemporals. By taking parameters $L = 1$, $v = 1$, $k = 0.5$, $\alpha = 0.5$, $R_1 = 0.3$, $\omega = 0.4$, $m = 0.5$, and $n = 0.5$, the plot's symmetric, recurring shapes suggest the existence of periodic bright soliton structures, which might be breather-like or multi-peak solutions.

Table 1. Compared to previously reported results.

Research	Solution type	Method used	Bifurcation analysis	Modulation instability	Sensitivity analysis
This work	Dark, bright, periodic multi-peaks breather-type	F-expansion, EMETEM	✓	✓	✓
[18]	Bright and dark soliton	Kudryashov's method, Sine-Gordon method	×	×	×
[35]	Bright and dark soliton	Laplace substitution method	×	×	×
[36]	Two-soliton	Hirota method	×	×	×
[37]	Periodic and kink solutions	Tanh-coth and sine-cosine methods	×	×	×

6. Bifurcation analysis

This section presents a comprehensive bifurcation analysis of the governing nonlinear equation. We begin by transforming the original system into a NLODE represented by Eq (2.5), utilizing the traveling wave transformation introduced earlier. Through this transformation and subsequent mathematical manipulation, we derive the following planar dynamical system that forms the foundation of our bifurcation analysis:

$$\begin{cases} N' = p, \\ p' = \frac{-\alpha N - 2k^2\beta N p^2}{ck + \beta k^2 N^2}. \end{cases} \tag{6.1}$$

It is noteworthy that the system under investigation does not exhibit Hamiltonian characteristics. From system (6.1), we derive

$$\frac{dp^2}{dN} = \frac{-2\alpha N - 4k^2\beta N p^2}{ck + \beta k^2 N^2}. \tag{6.2}$$

Since the singular point of Eq (6.2) occurs at $p = 0$, we observe that p vanishes only under specific parametric conditions. Solving Eq (6.2) yields

$$p^2 = \frac{-a_3}{a_4} + \left[a_2 N^2 + a_1\right]^{\frac{a_4}{2a_3}} c_1, \tag{6.3}$$

where $a_1 = ck^2$, $a_2 = \beta k^2$, $a_3 = -\alpha$, $a_4 = 2k^2\beta$, and c_1 represents an integration constant. This enables us to establish the corresponding conserved quantity

$$H(N, p) = p^2 - \left[\frac{-a_3}{a_4} + \left(a_2 N^2 + a_1\right)^{\frac{a_4}{2a_3}} c_1\right]. \tag{6.4}$$

The autonomous nature of Eq (6.4) ensures that the complete phase portrait consists exclusively of the system's contour lines. We proceed with a qualitative analysis using the complete discrimination method based on the previously established model. The potential energy embedded in Eq (6.4) takes the form

$$N = -\left[\frac{-a_3}{a_4} + \left(a_2 N^2 + a_1\right)^{\frac{a_4}{2a_3}} c_1\right], \tag{6.5}$$

and furthermore,

$$N' = -\left[-\frac{2\left(a_2 N^2 + a_1\right)^{-\frac{a_3}{a_2}} a_3 c_1 p}{a_2 N^2 + a_1}\right], \tag{6.6}$$

and then, setting $\frac{-a_3}{a_2} = 2$, we obtain

$$N' = -\left[-2a_2 a_3 c_1 p^3 - 2a_1 a_3 c_1 N\right]. \tag{6.7}$$

It is crucial to remember that the denominator in system (6.1) may result in singularities at certain points. In the following derivations, these singularities have been methodically eliminated to

guarantee that the dynamical system stays well-defined and appropriate for bifurcation analysis (Eqs (6.2)–(6.5)). The regularized form guarantees that the phase portraits faithfully depict the qualitative dynamics and bifurcation structures of the system, as bifurcation cannot take place at places where the system becomes undefined. Let $J(N, p)$ denote the linearized coefficient matrix at (N, p), conventionally referred to as the system's Jacobian matrix. The determinant of this Jacobian matrix is expressed as:

$$J(N, p) = \begin{vmatrix} 0 & 1 \\ -6c_1N^2a_2a_3 - 2a_1a_3c_1 & 0 \end{vmatrix}, \tag{6.8}$$

resulting in

$$J(N, p) = 6c_1N^2a_2a_3 + 2a_1a_3c_1. \tag{6.9}$$

The classification of critical points follows standard criteria: A cusp occurs when $J(N, 0) = 0$, a saddle manifests when $J(N, 0) < 0$, and a center point emerges when $J(N, 0) > 0$. Evaluating the polynomial discriminant

$$\Delta = -64a_1^3a_2a_3^4c_1^4, \tag{6.10}$$

we identify several distinctive cases characterized by different parameter configurations.
Case A: When $\Delta = 0$ with $c_1 > 0$; $a_1 = 0$; $a_2 > 0$; $a_3 > 0$, we have

$$N^{'} = (N - l)^3. \tag{6.11}$$

For parameter values $c_1 = 1$, $a_1 = 0$, $a_2 = 1$, and $a_3 = 1$, a single equilibrium point emerges at $(0, 0)$, exhibiting cusp behavior as illustrated in Figure 8.

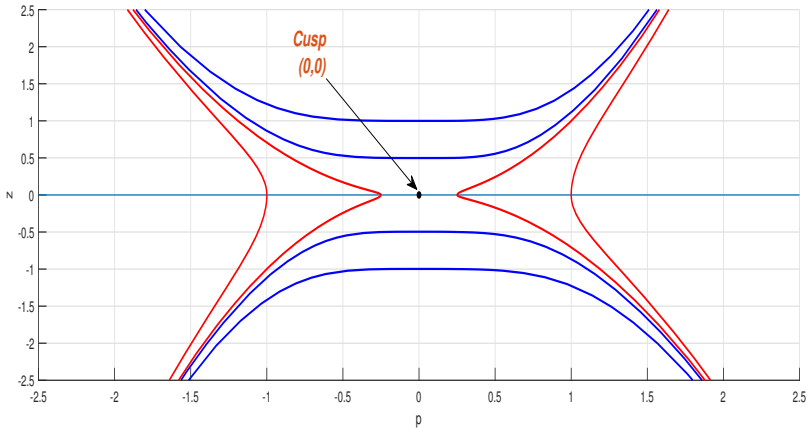

Figure 8. Global phase portrait for case A.

Case B: When $\Delta = 0$ with $c_1 > 0$; $a_1 > 0$; $a_2 = 0$; $a_3 > 0$, the system reduces to

$$N^{'} = N - l. \tag{6.12}$$

With parameter values $c_1 = 1$, $a_1 = 1$, $a_2 = 0$, and $a_3 = 1$, a single equilibrium point occurs at $(0, 0)$, classified as a center point, as depicted in Figure 9.

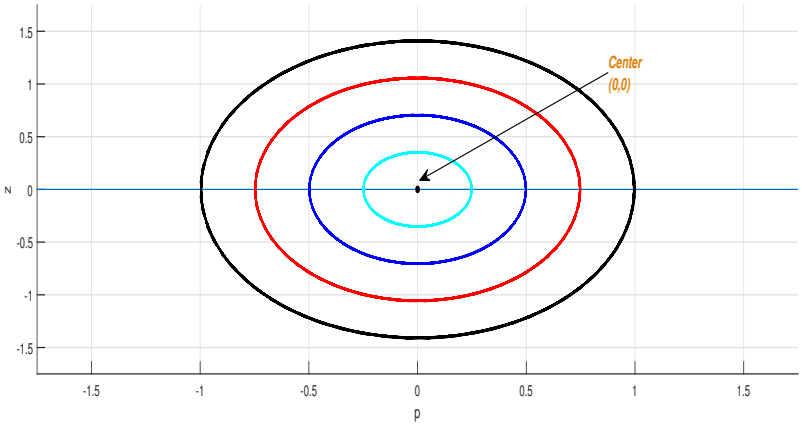

Figure 9. Global phase portrait for case B.

Case C: For $\Delta = 0$ with $c_1 > 0$; $a_1 > 0$; $a_2 = 0$; $a_3 < 0$, we obtain

$$N^{'} = N - s. \tag{6.13}$$

Under parameter conditions $c_1 = 1$, $a_1 = 1$, $a_2 = 0$, and $a_3 = -1$, a single equilibrium point exists at $(0, 0)$, characterized as a saddle point, as shown in Figure 10.

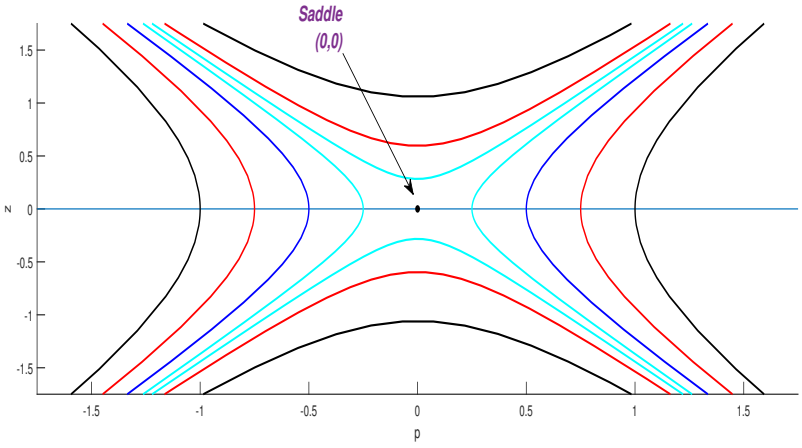

Figure 10. Global phase portrait for case C.

Case D: When $\Delta > 0$ with $c_1 > 0$; $a_1 > 0$; $a_2 < 0$; $a_3 > 0$, the system takes the form

$$p^{'} = (p - l)(p - m)(p - n). \tag{6.14}$$

This configuration yields three equilibrium points: $(l, 0)$, $(m, 0)$, and $(n, 0)$, where $(m, 0)$ functions as a center while $(l, 0)$ and $(n, 0)$ constitute saddle points. For parameter values $c_1 = 1$, $a_1 = 1$, $a_2 = -1$, and $a_3 = 1$, the equilibrium points are located at $l = -1$, $m = 0$, and $n = 1$, as illustrated in Figure 11.

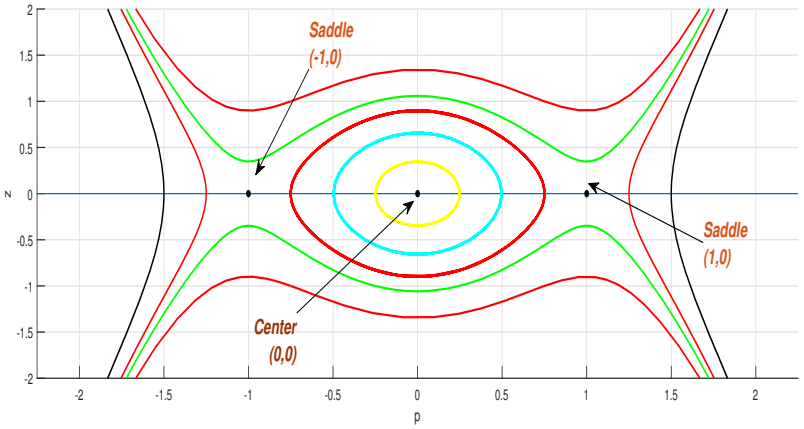

Figure 11. Global phase portrait for case D.

Case E: For $\Delta > 0$ with $c_1 > 0$; $a_1 < 0$; $a_2 > 0$; $a_3 > 0$, we have

$$N^{'} = (N - l)(N - m)(N - n). \tag{6.15}$$

This configuration generates three equilibrium points: $(l, 0)$, $(m, 0)$, and $(n, 0)$, where $(m, 0)$ functions as a saddle while $(l, 0)$ and $(n, 0)$ represent center points. For parameter values $c_1 = 1$, $a_1 = -1$, $a_2 = 1$, and $a_3 = 1$, the equilibrium points are positioned at $l = -1$, $m = 0$, and $n = 1$, as depicted in Figure 12.

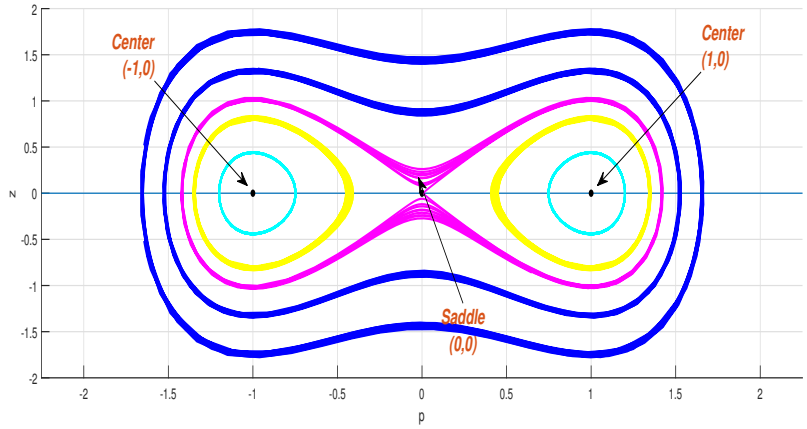

Figure 12. Global phase portrait for case E.

Case F: When $\Delta > 0$ with $c_1 > 0$; $a_1 < 0$; $a_2 < 0$; $a_3 > 0$, the system becomes

$$N^{'} = (N - l)(N - m)(N - n), \tag{6.16}$$

resulting in a single equilibrium point $(l, 0)$, which manifests as a saddle. For parameter values $c_1 = 1$, $a_1 = -1$, $a_2 = -1$, and $a_3 = 1$, the equilibrium point is positioned at $l = 0$, as shown in Figure 13.

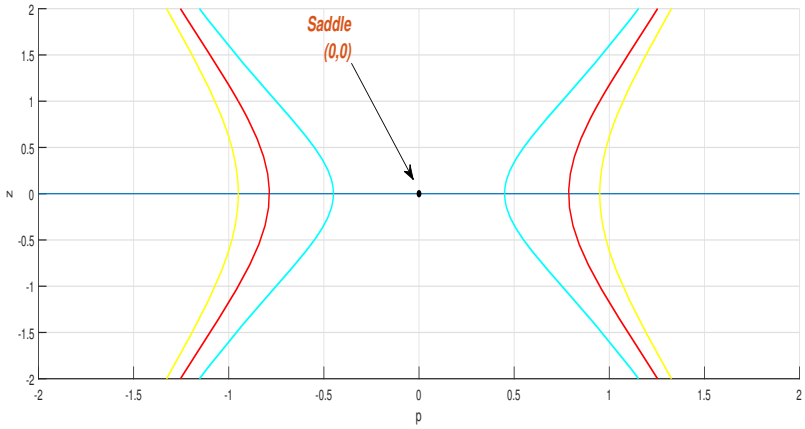

Figure 13. Global phase portrait for case F.

Case G: For $\Delta < 0$ with $c_1 > 0$; $a_1 > 0$; $a_2 > 0$; $a_3 > 0$, we obtain

$$N^{'} = (N - m)((N - l)^2 + n^2), \tag{6.17}$$

yielding a single equilibrium point $(m, 0)$, which functions as a center. For parameter values $c_1 = 1$, $a_1 = 1$, $a_2 = 1$, and $a_3 = 1$, the equilibrium point is located at $m = 0$, as illustrated in Figure 14.

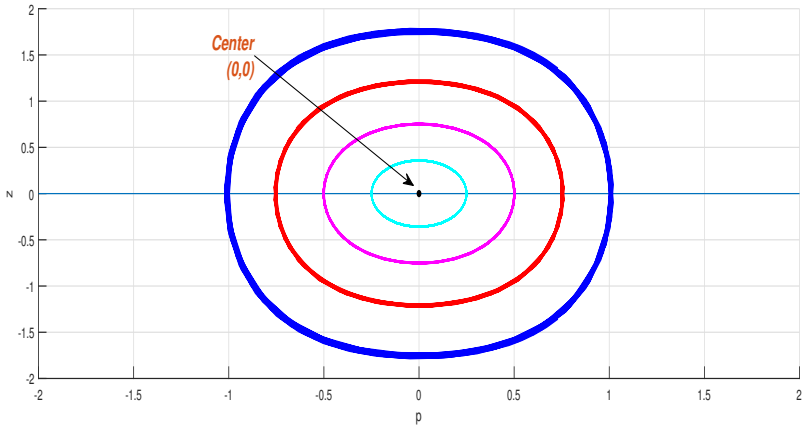

Figure 14. Global phase portrait for case G.

7. Modulation instability

This section examines modulation instability (MI) phenomena in higher-order nonlinear partial differential equations, focusing on perturbation-induced modifications to constant-state solutions through the interplay between nonlinear and dispersive effects. To analyze this behavior systematically, we express the perturbed equilibrium solution of Eq (2.2) in the form:

$$\psi = (P + \sigma R(x, t)), \tag{7.1}$$

where P represents the incident power, σ (with $\sigma \ll 1$) serves as the perturbation parameter, and R denotes the impact term quantifying the deviation from equilibrium. Substituting this representation

into Eq (2.2) and performing a linearization with respect to R, we obtain:

$$\beta\sigma P^2 R_x - \alpha P - \alpha\sigma R + \sigma R_{tx} = 0. \tag{7.2}$$

To investigate the instability characteristics, we analyze solutions that exhibit exponential growth of the form:

$$R(x,t) = p_1 e^{i(kx-\omega t)} + p_2 e^{-i(kx-\omega t)}, \tag{7.3}$$

where p_1 and p_2 are amplitude coefficients, while k and ω represent the wave number and frequency, respectively. Inserting this ansatz into Eq (7.2) yields the following system of homogeneous equations:

$$\begin{aligned}\beta\sigma P^2 p_1 k^2 + \sigma p_1 \omega k - \alpha\sigma p_1 = 0,\\ \beta\sigma P^2 p_2 k^2 + \sigma p_2 \omega k - \alpha\sigma p_2 = 0.\end{aligned}$$

Solving this system produces the dispersion relation

$$\omega = \pm\left(\frac{-\beta k^2 P^2 + \alpha}{k}\right). \tag{7.4}$$

Stability analysis of the equilibrium state defined by Eq (7.4) reveals that when ω remains real-valued, the steady-state solution maintains stability. Conversely, when ω develops an imaginary component, the equilibrium becomes unstable as perturbations grow exponentially over time. The modulation instability gain spectrum is consequently determined by

$$\begin{aligned} g(k) &= 2\mathrm{Im}(\omega),\\ &= 2\mathrm{Im}\left(\frac{-\beta k^2 P^2 + \alpha}{k}\right). \end{aligned} \tag{7.5}$$

The expression in Eq (7.4) shows that the frequency ω becomes complex-valued when the quantity $-\beta k^2 P^2 + \alpha$ is complex or changes sign. This implies that instability arises when $\beta k^2 P^2 > \alpha$, leading to a positive imaginary part of ω. Thus, the MI gain spectrum is non-zero only in a specific range of wave numbers k, bounded by:

$$k \in \left(0, \sqrt{\frac{\alpha}{\beta P^2}}\right). \tag{7.6}$$

This range defines the instability band where perturbations grow exponentially.

This analysis demonstrates that the magnitude of the MI gain is significantly influenced by the incident strength parameter σ. Additionally, the MI gain exhibits sensitivity to nonlinear effects, detuning parameters, and group velocity dispersion. These relationships are graphically illustrated in Figure 15, which depicts the modulation instability gain spectrum under various parametric conditions. The gain spectrum in Figure 15 is analytically obtained from Eq (7.4), not from direct numerical simulation of Eq (2.2). This allows parametric understanding of how MI varies with system parameters.

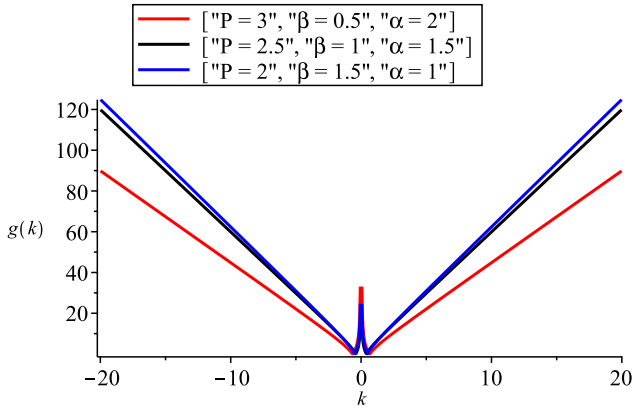

Figure 15. Modulation instability gain spectrum $g(k)$ versus wavenumber k for the SWE for varying values of P, α, and β. The instability region appears within a finite band of k where the imaginary part of ω becomes positive, indicating exponential growth. The maximum gain occurs at a finite k corresponding to optimal perturbation. The red curve represents $P = 3$, $\beta = 0.5$, $\alpha = 2$; the black curve corresponds to $P = 2.5$, $\beta = 1$, $\alpha = 1.5$; and the blue curve shows $P = 2$, $\beta = 1.5$, $\alpha = 1$. The graph illustrates how the MI gain profile varies with incident power, nonlinearity, and dispersion parameters, displaying a characteristic V-shaped pattern with a singularity near $k = 0$.

8. Sensitivity analysis

This section examines the sensitivity analysis of the proposed model. Sensitivity analysis of dynamical models provides valuable insights into system behavior, aids in model validation and calibration, quantifies uncertainty, and improves risk assessment and management. It also influences decisions regarding control and optimization strategies. The sensitivity analysis shows how little changes to important parameters have a big impact on the stability and structure of the resulting solutions. This phenomenon has immediate applications, such as in nonlinear optics or fluid dynamics, where even little input or ambient variations may significantly alter the way waves propagate. Designing more stable systems, enhancing control schemes, and more precisely forecasting wave behavior under disturbances are all made easier with an understanding of this sensitivity. For the SWE, sensitivity analysis determines how minor adjustments or perturbations to the equation's parameters or initial conditions affect its solutions.

Equation (2.5) can be transformed into two distinct systems through Galilean transformation. To investigate the parametric sensitivities of this dynamical system represented by Eq (6.1), we employ the widely established Runge–Kutta computational integration scheme. The quantitative analysis evaluates the following coupled differential model:

$$\begin{cases} N' = p, \\ p' = \frac{-aN - 2k^2\beta N p^2}{ck + \beta k^2 N^2}. \end{cases} \tag{8.1}$$

To systematically examine the sensitivity characteristics, we consider two distinct sets of initial conditions:

- Set 1: $(N(0), p(0)) = (0.1, 0.15)$, $(0.1, 0.35)$, and $(0.1, 0.55)$,
- Set 2: $(N(0), p(0)) = (0.02, 0.25)$, $(0.02, 0.45)$, and $(0.02, 0.65)$.

The numerical results shown by Figure 16 demonstrate that small perturbations in initial conditions can induce significant variations in the dynamic evolution of the solutions, indicating high sensitivity to initial state configurations. While this section investigates sensitivity to initial conditions, a complementary analysis involving global parameter perturbations (e.g., Sobol index-based uncertainty quantification for α, β, and k) remains an important direction for extending the present model's applicability.

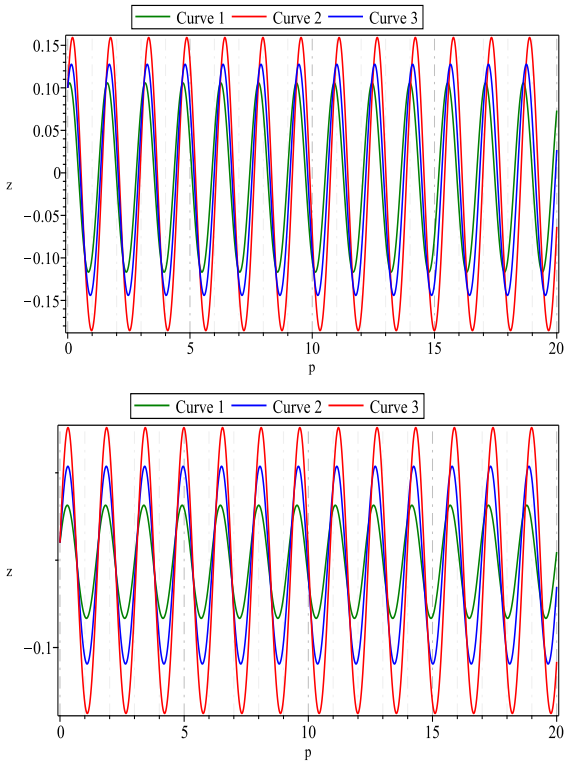

Figure 16. Sensitivity analysis of the differential system with parameters $\alpha = -1$, $\beta = -2$, $k = 0.2$, and $c = 0.3$: (a) Trajectory evolution for set 1 initial conditions showing divergent behavior over time; (b) Dynamic response for Set 2 initial conditions demonstrating phase space trajectory sensitivity.

9. Conclusions

This work presents a systematic analytical study of the Schäfer-Wayne equation modeling ultra-short pulse propagation in nonlinear optical fibers. Using the F-expansion and enhanced modified extended tanh expansion methods, we derived a variety of soliton solutions, namely, bright, dark, singular, and periodic, and analyzed their structural properties and stability through bifurcation, modulation instability, and sensitivity analyses. To elucidate the qualitative properties of the system, we applied a Galilean transformation to convert the equation into a planar dynamical system, enabling the classification of all possible phase portraits through complete discrimination analysis. A detailed

sensitivity analysis confirmed the model's robustness while identifying critical parameter thresholds, and the phase amplitude ansatz method yielded exact bright and dark solitary wave solutions. Significantly, we demonstrated that both solution types can coexist in the anomalous dispersion regime, subject to specific parameter constraints. Additionally, our modulation instability analysis revealed its fundamental role as a precursor to soliton formation, providing essential insights into the wave stability mechanisms.

In particular, the bright soliton solution (see Eq (4.6)) exhibits a cn/sech profile similar to soliton solution of nonlinear Schrödinger equaion used in optical pulse compression. NLSE-based systems typically achieve compression ratios of 5–10× over 100 km in dispersion-managed fibers [40]. Given the structural similarity, Eq (4.6) is expected to offer comparable potential, pending numerical validation with realistic fiber parameters. These findings provide a theoretical foundation for soliton-based technologies in long-haul communications, optical switching, and sensing applications.

Future research directions encompass extending analytical methodologies to higher-order, fractional, and perturbed versions of the SW model, and applying these techniques to other physically relevant integrable systems. We hope to explore the SWE by finding higher-order soliton and other solutions like breather, rogue wave, positon, and breather-positon (b-positon) solutions by using Darboux transformation [41, 42] and inverse scattering methods. Future work can also focus on numerical simulations incorporating fiber loss, higher-order dispersion, and Raman effects to validate the compression performance of SWE solitons over long-haul fiber links, and to compare quantitatively with NLSE solitons.

Author contributions

Maha Alammari: Formal analysis, validation, methodology, investigation, writing-review & editing. Muhammad Abuzar: Software, investigation, writing-review & editing. Solomon Manukure: Writing-review & editing, supervision, resources. All authors have read and approved the final version of the manuscript for publication.

Use of Generative-AI tools declaration

The authors declare that they have not used Artificial Intelligence tools in the creation of this article.

Acknowledgement

We sincerely appreciate the reviewers for their valuable comments and constructive feedback, which have significantly contributed to improving the quality of this manuscript.

Conflict of interest

All authors declare no conflicts of interest in this paper.

References

1. U. Demirbilek, A. H. Tedjani, A. R. Seadawy, Analytical solutions of the combined Kairat-II-x equation: A dynamical perspective on bifurcation, chaos, energy, and sensitivity, *AIMS Mathematics*, **10** (2025), 13664–13691. https://doi.org/10.3934/math.2025615
2. S. Manukure, T. Booker, A short overview of solitons and applications, *Partial Differ. Equ. Appl. Math.*, **4** (2021), 100140. https://doi.org/10.1016/j.padiff.2021.100140
3. N. Akhmediev, M. Karlsson, Cherenkov radiation emitted by solitons in optical fibers, *Phys. Rev. A.*, **51** (1995), 2602. https://doi.org/10.1103/PhysRevA.51.2602
4. H. Ma, R. U. Rahman, S. Manukure, Dynamical analysis and bifurcations in a fractional integrable equation, *Alex. Eng. J.*, **125** (2025), 600–623. https://doi.org/10.1016/j.aej.2025.03.138
5. M. Junjua, A. M. Mostafa, N. F. AlQahtani, A. Bekir, Impact of truncated M-fractional derivative on the new types of exact solitons to the (4+1)-dimensional DSKP model, *Mod. Phys. Lett. B*, **38** (2024), 2450313. https://doi.org/10.1142/S0217984924503135
6. A. K. Alsharidi, M. Junjua, Kink, dark, bright, and singular optical solitons to the space–time nonlinear fractional (4+1)-dimensional Davey–Stewartson–Kadomtsev–Petviashvili model, *Fractal Fract.*, **8** (2024), 388. https://doi.org/10.3390/fractalfract8070388
7. M. A. Alomair, M. Junjua, Analysis of truncated M-fractional mathematical and physical (2+1)-dimensional nonlinear Kadomtsev–Petviashvili-modified equal-width model, *Fractal Fract.*, **8** (2024), 442. https://doi.org/10.3390/fractalfract8080442
8. W. B. Rabie, H. M. Ahmed, T. A. Nofal, S. Alkhatib, Wave solutions for the (3+1)-dimensional fractional Boussinesq-KP-type equation using the modified extended direct algebraic method, *AIMS Mathematics*, **9** (2024), 31882–31897. https://doi.org/10.3934/math.20241532
9. N. Raza, R. Ur Rahman, A. Seadawy, A. Jhangeer, Computational and bright soliton solutions and sensitivity behavior of Camassa–Holm and nonlinear Schrödinger dynamical equation, *Int. J. Mod. Phys. B*, **35** (2021), 2150157. https://doi.org/10.1142/S0217979221501575
10. A. H. Arnous, Chaotic dynamics and bifurcation analysis of optical solitons in birefringent fibers governed by the Sasa-Satsuma equation with stochastic perturbation, *Nonlinear Dyn.*, **113** (2025), 18469–18484. https://doi.org/10.1007/s11071-025-11107-1
11. I. Samir, H. M. Ahmed, W. Rabie, W. Abbas, O. Mostafa, Construction optical solitons of generalized nonlinear Schrödinger equation with quintuple power-law nonlinearity using Exp-function, projective Riccati, and new generalized methods, *AIMS Mathematics*, **10** (2025), 3392–3407. https://doi.org/10.3934/math.2025157
12. S. S. Miah, M. A. Akbar, K. Khan, Solitary wave solutions and stability analysis of the fractional Sawada-Kotera equation using the extended modified auxiliary equation mapping method, *J. Umm Al-Qura Univ. Appl. Sci.*, 2025. https://doi.org/10.1007/s43994-025-00230-9
13. N. Raza, A. Jhangeer, R. Ur Rahman, A. R. Butt, Y. M. Chu, Sensitive visualization of the fractional Wazwaz-Benjamin-Bona-Mahony equation with fractional derivatives: A comparative analysis, *Results Phys.*, **25** (2021), 104171. https://doi.org/10.1016/j.rinp.2021.104171

14. I. Hamid, S. Kumar, Newly formed solitary wave solutions and other solitons to the (3+1)-dimensional mKdV–ZK equation utilizing a new modified Sardar sub-equation approach, *Mod. Phys. Lett. B*, **39** (2025), 2550027. https://doi.org/10.1142/S0217984925500277

15. D. Kumar, A. Saharan, A. Kumar, Exploring soliton patterns and dynamical analysis of the solitary wave form solutions of the (3+1)-dimensional Wazwaz–Benjamin–Bona–Mahony equation, *Mod. Phys. Lett. B*, **39** (2025), 2550102. https://doi.org/10.1142/S0217984925501027

16. H. W. A. Riaz, J. Lin, Darboux transformation for a semi-discrete matrix coupled dispersionless system, *Appl. Math. Lett.*, **158** (2024), 109217. https://doi.org/ 10.1016/j.aml.2024.109217

17. R. Ur Rahman, Z. Li, J. He, Magnetic wave dynamics in ferromagnetic thin films: Interactions of solitons and positons in Landau-Lifshitz-Gilbert equation, *Physica D*, **479** (2025), 134719. https://doi.org/10.1016/j.physd.2025.134719

18. K. K. Ali, A. Saha, M. N. Ali, T. Ak, M. M. A. Khater, Dynamical properties of Schäfer-Wayne equation for propagation of short pulses in silica optical fibers, *Opt. Quant. Electron.*, **56** (2024), 1334. https://doi.org/10.1007/s11082-024-07238-1

19. B. F. Feng, L. Ling, Z. Zhu, Defocusing complex short-pulse equation and its multi-dark-soliton solution, *Phys. Rev. E*, **93** (2016), 052227. https://doi.org/10.1103/PhysRevE.93.052227

20. H. W. A. Riaz, M. Ul Hassan, On soliton solutions of multi-component semi-discrete short pulse equation, *J. Phys. Commun.*, **2** (2018), 025005. https://doi.org/10.1088/2399-6528/aaa4e1

21. V. Kumar, A. Biswas, M. Ekici, L. Moraru, A. K. Alzahrani, M. R. Belic, Time–dependent coupled complex short pulse equation: Invariant analysis and complexitons, *Chaos Soliton. Fract.*, **150** (2021), 111151. https://doi.org/10.1016/j.chaos.2021.111151

22. D. Zhao, Zhaqilao, On two new types of modified short pulse equation, *Nonlinear Dyn.*, **100** (2020), 615–627. https://doi.org/10.1007/s11071-020-05530-9

23. V. K. Kuetche, T. B. Bouetou, T. C. Kofane, On two-loop soliton solution of the Schäfer-Wayne short-pulse equation using Hirota's method and Hodnett-Moloney approach, *J. Phys. Soc. Jpn.*, **76** (2007), 024004. https://doi.org/10.1143/JPSJ.76.024004

24. A. Sakovich, S. Sakovich, Solitary wave solutions of the short pulse equation, *J. Phys. A: Math. Gen.*, **39** (2006), L361. https://doi.org/10.1088/0305-4470/39/22/L03

25. Y. Chung, C. K. R. T. Jones, T. Schäfer, C. E. Wayne, Ultra-short pulses in linear and nonlinear media, *Nonlinearity*, **18** (2005), 1351. https://doi.org/10.1088/0951-7715/18/3/021

26. D. Ampilogov, S. Leble, Evolution equation for interaction of opposite directed waves with arbitrary polarization in 1D-metamaterial, *J. Nonlinear Opt. Phys. Mater.*, **31** (2022), 2150013. https://doi.org/10.1142/S0218863521500132

27. J. Xu, N. Guo, H. Li, Y. Tu, On the double-pole solutions of the complex short-pulse equation, *Mod. Phys. Lett. B*, **35** (2021), 2150129. https://doi.org/10.1142/S0217984921501293

28. H. Esen, M. Ozisik, A. Secer, M. Bayram, Optical soliton perturbation with Fokas-Lenells equation via enhanced modified extended tanh-expansion approach, *Optik*, **267** (2022), 169615. https://doi.org/10.1016/j.ijleo.2022.169615

29. J. L. Zhang, M. L. Wang, Y. M. Wang, Z. D. Fang, The improved F-expansion method and its applications, *Phys. Lett. A*, **350** (2006), 103–109. https://doi.org/10.1016/j.physleta.2005.10.099

30. M. A. Akbar, N. H. M. Ali, The improved F-expansion method with Riccati equation and its applications in mathematical physics, *Cogent Math.*, **4** (2017), 1282577. https://doi.org/10.1080/23311835.2017.1282577

31. M. M. A. Khater, A. Jhangeer, H. Rezazadeh, L. Akinyemi, M. A. Akbar, M. Inc, Propagation of new dynamics of longitudinal bud equation among a magneto-electro-elastic round rod, *Mod. Phys. Lett. B*, **35** (2021), 2150381. https://doi.org/10.1142/S0217984921503814

32. R. Ur Rahman, Z. Hammouch, A. S. A. Alsubaie, K. H. Mahmoud, A. Alshehri, E. A. Az-Zo'bi, et al., Dynamical behavior of fractional nonlinear dispersive equation in Murnaghan's rod materials, *Results Phys.*, **56** (2024), 107207. https://doi.org/10.1016/j.rinp.2023.107207

33. J. C. Brunelli, The short pulse hierarchy, *J. Math. Phys.*, **46** (2005), 123507. https://doi.org/10.1063/1.2146189

34. A. Sakovich, S. Sakovich, The short pulse equation is integrable, *J. Phys. Soc. Jpn.*, **74** (2005), 239–241. https://doi.org/10.1143/JPSJ.74.239

35. O. Gonzalez-Gaxiola, Bright and dark optical solitons of the Schäfer–Wayne short-pulse equation by Laplace substitution method, *Optik*, **200** (2020), 163414. https://doi.org/10.1016/j.ijleo.2019.163414

36. V. K. Kuetche, T. B. Bouetou, T. C. Kofane, On two-loop soliton solution of the Schäfer–Wayne short-pulse equation using Hirota's method and Hodnett–Moloney approach, *J. Phys. Soc. Jpn.*, **76** (2007), 024004. https://doi.org/10.1143/JPSJ.76.024004

37. T. Schäfer, C. E. Wayne, Propagation of ultra-short optical pulses in cubic nonlinear media, *Physica D*, **196** (2004), 90–105. https://doi.org/10.1016/j.physd.2004.04.007

38. W. Blanc, B. Dussardier, Formation and applications of nanoparticles in silica optical fibers, *J. Opt.*, **45** (2016), 247–254. https://doi.org/10.1007/s12596-015-0281-6

39. Y. Shen, N. Whitaker, P. G. Kevrekidis, N. L. Tsitsas, D. J. Frantzeskakis, Ultrashort pulses and short-pulse equations in 2+1 dimensions, *Phys. Rev. A*, **86** (2012), 023841. https://doi.org/10.1103/PhysRevA.86.023841

40. G. Agrawal, *Nonlinear fiber optics*, 5 Eds, Berlin: Springer, 2013. https://doi.org/10.1016/C2011-0-00045-5

41. H. W. A. Riaz, J. Lin, J. Wang, On an extended semi-discrete matrix coupled dispersionless system: Darboux transformation and explicit solutions, *Phys. Lett. A*, **528** (2024), 130060. https://doi.org/10.1016/j.physleta.2024.130060

42. H. W. A. Riaz, Quasi-Wronskian solitons in the non-commutative kuralay-IIA equation: Analysis and simulations, *Phys. Scr.*, **100** (2025), 025239. https://doi.org/10.1088/1402-4896/ada4ee

AIMS Press